*Journal of Sound and Vibration* (1999) **223**(2), 297–316
*Article No*. jsvi.1998.2095, available online at http://www.idealibrary.com on IDEAL®

# COUPLED BENDING TORSIONAL VIBRATION OF ROTORS USING FINITE ELEMENT

M. A. Mohiuddin and Y. A. Khulief

*Department of Mechanical Engineering, King Fahd University of Petroleum & Minerals, KFUPM P.O. Box* 1767, *Dhahran* 31261, *Saudi Arabia*

(*Received* 17 *January* 1996, *and in final form* 17 *December* 1998)

A finite element formulation of the dynamic model of a rotor-bearing system is presented. The elastodynamic model of coupled bending and torsional motions of the rotating shaft is derived using the Lagrangian approach. The model accounts for the gyroscopic effects as well as the inertia coupling between bending and torsional deformations. A reduced order model is obtained using modal truncation. The modal transformation invokes the complex mode shapes of a general rotor system with gyroscopic effects and anisotropic bearings. The reduced modal form of the dynamic model is numerically simulated, and the dynamic responses due to different excitations are obtained.



## 1. INTRODUCTION

Rotating machines are extensively used in diverse engineering applications, such as power stations, marine propulsion systems, aircraft engines, machine tools, automobiles, medical equipment and household accessories. The dynamic modelling of such systems is essential to understand their dynamic behavior and the associated vibration problems.

Although early dynamic models of rotor systems were formulated either analytically [1] or using the transfer matrix approach [2], the potential of the powerful finite element technique was recognized at a very early stage [3]. Nelson and McVaugh [4] and Zorzi and Nelson [5] improved upon the model presented in reference [3] by including secondary effects such as rotary inertia, internal damping and axial torque. Several finite element formulations using a uniform shaft element [6, 7] or tapered shaft element [8–11] were introduced to evaluate the modal characteristics of rotor-bearing systems.

For dynamic response analysis, a linearized finite element model was employed to establish a control scheme for rotor systems [12]. The finite element method was also applied to a complex rotor system to evaluate its vibration response due to fluid forces [13], and gyroscopic moments [14]. General purpose finite element codes [15] were adapted to simulate the dynamics of some complex

0022–460X/99/220297 + 20 $30.00/0 

rotor systems. The coupling between the bending and torsional deformations, however, was not included in the previously cited dynamic response analyses.

All of the reported finite element dynamic analysis studies were based on the utilization of the nodal or physical co-ordinates. The use of nodal co-ordinates, however, results in a large dimensionality, thus inhibiting the efficiency of the numerical solution. Although reduced order finite element models using modal co-ordinates were introduced for flexible multibody dynamic analysis [16–18], they were not adopted for dynamic analysis of rotor-bearing systems.

Kane and Torby [19] referred to the different methods for reducing the size of the finite element model while preserving the lower frequencies. They introduced a modal transformation that resulted in reduced mass and stiffness matrices, and showed that the reduced model preserves the same modal characteristics of the original finite element model. Their work, however, was not carried out to the dynamic response analysis stage.

In this paper, a finite element elastodynamic model of a rotor-bearing system is formulated. The model accounts for the gyroscopic effects, as well as the coupling between flexural and torsional deformations. In addition, the formulation permits the use of either a uniform or tapered shaft element, and general anisotropic bearings. A modal transformation utilizing the complex mode shapes is established, and a reduced order model is obtained. The reduced modal form of the equations of motion is numerically generated and integrated forward in time. The dynamic response is obtained for some numerical examples to demonstrate the validity and efficiency of the developed model.

## 2. THE ELASTODYNAMIC MODEL OF THE ROTOR

Two reference frames are employed to describe the motion of the rotor system. One is the fixed reference $XYZ$, and the other is a rotating reference $xyz$. The $X$- and $x$-axes are colinear and coincident with the undeformed rotor centerline. The angular displacement between the two reference frames is $\theta(t)$, and the rotational speed of the shaft is defined by $\dot{\theta}(t)$.

In this formulation, it is assumed that: (1) the material of the rotor is elastic, homogeneous and isotropic; (2) the plane cross-sections initially perpendicular to the neutral axis of the rotor remain plane, but no longer perpendicular to the neutral axis during bending; (3) the deflection of the rotor is produced by the displacement of points of the center line; (4) the axial motion of the rotor is small and can be neglected; (5) the shaft is flexible, while disks are treated as rigid; and (6) internal damping and aerodynamic forces are neglected.

### 2.1. THE ELEMENTAL CO-ORDINATE SYSTEM OF THE SHAFT

The finite element method is used to model the shaft. Referring to Figure 1, let $X^iY^iZ^i$ be a Cartesian co-ordinate system with its origin fixed to the undeformed shaft element. $x^iy^iz^i$ is a Cartesian co-ordinate system after the deformation of the shaft element. The $x^iy^iz^i$ co-ordinate system is rotated with respect to the $X^iY^iZ^i$ co-ordinate system through a set of angles $\phi$, $\beta$ and $\gamma$, as shown in Figure 2. To describe the general orientation of any cross-section of the shaft element,

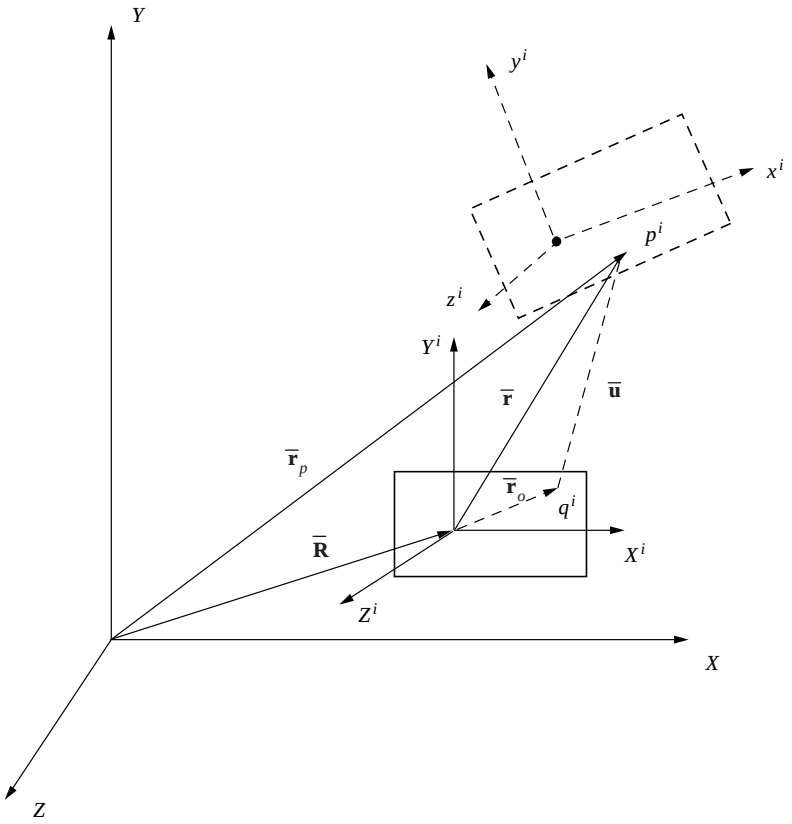


Figure 1. Generalized co-ordinates of the $i$th element.

one first rotates it by an angle $(\theta + \phi)$ around the $X^i$-axis, then an angle $\beta$ around the new $y^i$-axis (denoted by $y_2^i$), and finally by an angle $\gamma$ around the final $z^i$-axis. The instantaneous angular velocity vector of the $x^i y^i z^i$ frame may be expressed as

$$\bar{\omega} = (\dot{\theta} + \dot{\phi})\hat{\mathbf{I}} + \dot{\beta}\hat{\mathbf{j}}_2 + \dot{\gamma}\hat{\mathbf{k}}, \tag{1}$$

where $\hat{\mathbf{I}}$, $\hat{\mathbf{j}}_2$ and $\hat{\mathbf{k}}$ are unit vectors along the axes $X$, $y_2^i$ and $z^i$.

### 2.2. KINETIC ENERGY OF THE SHAFT

Referring to Figure 1, let $q^i$ be any point in the undeformed shaft element $i$. Point $p^i$ is defined by the vector $\bar{\mathbf{r}}_o$, with respect to the $X^i Y^I Z^i$ co-ordinate system. Point $q^i$ is then transformed to point $p^i$ in the deformed state of the shaft element. The location of $p^i$ with respect to the $X^i Y^I Z^i$ co-ordinate system is given by the vector $\bar{\mathbf{r}}$, and its global position is defined by the vector $\bar{\mathbf{r}}_p$, where, for simplicity of notation, the superscript $i$ is dropped when writing the position vector. One can write the position vector $\bar{\mathbf{r}}_p$ of point $p^i$ as

$$\bar{\mathbf{r}}_p = \bar{\mathbf{R}} + \bar{\mathbf{r}} = \bar{\mathbf{R}} + \bar{\mathbf{r}}_o + \bar{\mathbf{u}}, \tag{2}$$

where $\bar{\mathbf{R}}$ defines the location of the origin of the $X^i Y^I Z^i$ system with respect to

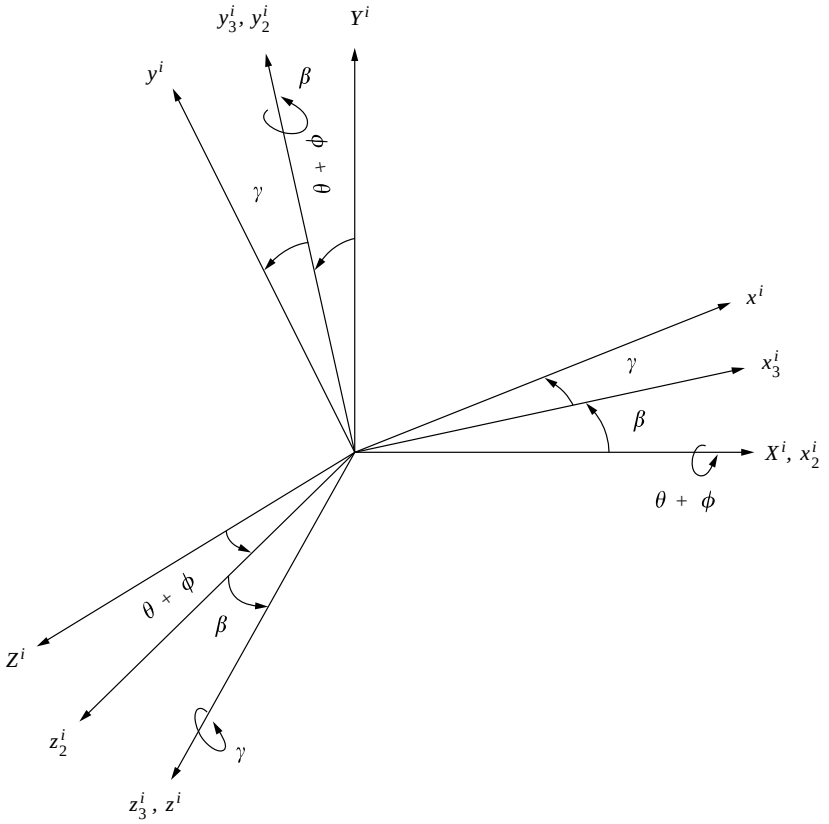


Figure 2. Cross-section rotation angles.

the global co-ordinate system $XYZ$ and $\bar{\mathbf{u}}$ represents the deformation vector of point $p^i$. Differentiating $\bar{\mathbf{r}}_p$ with respect to time and using the finite element analysis, the velocity of point $p^i$ can be written in matrix form as

$$\frac{\mathrm{d}\bar{\mathbf{r}}_p}{\mathrm{d}t} = [\mathbf{N}_v]\{\dot{\mathbf{e}}\} + [\tilde{\boldsymbol{\omega}}]\{\mathbf{r}_p\} = [\mathbf{N}_v \quad \tilde{\boldsymbol{\omega}}]\begin{bmatrix}\dot{\mathbf{e}}\\ \mathbf{r}_p\end{bmatrix}, \tag{3}$$

where $\{\mathbf{e}\}$ is the vector of nodal co-ordinates of the $i$th shaft element, and $[\mathbf{N}_v]$ is the translation shape function. The kinetic energy of the element is obtained by integrating the kinetic energy of an infinitesimal volume at point $p$ over the volume $V$. This can be written as

$$\begin{aligned} T &= \frac{1}{2}\int_V \mu\left\{\frac{\mathrm{d}\bar{\mathbf{r}}_p}{\mathrm{d}t}\right\}^t\left\{\frac{\mathrm{d}\bar{\mathbf{r}}_p}{\mathrm{d}t}\right\}\mathrm{d}V \\ &= \frac{1}{2}\int_V \mu[\{\dot{\mathbf{e}}\}^t[\mathbf{N}_v]^t[\mathbf{N}_v]\{\dot{\mathbf{e}}\} + \{\dot{\mathbf{e}}\}^t[\mathbf{N}_v]^t[\tilde{\boldsymbol{\omega}}]\{\mathbf{r}_p\} \\ &\quad + \{\mathbf{r}_p\}^t[\tilde{\boldsymbol{\omega}}]^t[\mathbf{N}_v]\{\dot{\mathbf{e}}\} + \{\mathbf{r}_p\}^t[\tilde{\boldsymbol{\omega}}]^t[\tilde{\boldsymbol{\omega}}]\{\mathbf{r}_p\}]\,\mathrm{d}V, \end{aligned} \tag{4}$$

where $\mu$ is the mass density of the shaft element number $i$. It is noted that

although we are describing element number $i$, the superscript $i$ is dropped. The first term in equation (4) gives the kinetic energy due to translation, the second and third terms are identically zero if moments of intertia are calculated with respect to the center of mass of the element. The last term gives the kinetic energy due to rotational effects that include gyroscopic moments. Equation (4) can be expressed as

$$T = \frac{1}{2}\{\dot{\mathbf{e}}\}^t[\mathbf{M}]\{\dot{\mathbf{e}}\} + \frac{1}{2}C^*\dot{\theta}^2 - \dot{\theta}\{\dot{\mathbf{e}}\}^t[\mathbf{G}^*]\{\mathbf{e}\}, \tag{5}$$

where

$$[\mathbf{M}] = [\mathbf{M}_t] + [\mathbf{M}_r] + [\mathbf{M}_\phi] - 2[\mathbf{M}_e]$$

is the composite mass matrix. The matrix $[\mathbf{M}_e]$ represents the coupling between torsional and transverse vibration, and is time dependent because it is a function of the nodal co-ordinates $\{\mathbf{e}\}$. Since the coupling terms which are time dependent are present in the inertia matrix, the coupling is called inertial coupling. The constituent matrices of $[\mathbf{M}]$ and other invariants in equation (5) are defined as

$$[\mathbf{M}_t] = \int_0^l [\mathbf{N}_v]^t \mu A [\mathbf{N}_v]\, \mathrm{d}x, \quad [\mathbf{M}_r] = \int_0^l [\mathbf{N}_\beta]^t I_D [\mathbf{N}_\beta]\, \mathrm{d}x,$$

$$[\mathbf{M}_\phi] = \int_0^l [\mathbf{N}_\phi]^t I_P [\mathbf{N}_\phi]\, \mathrm{d}x, \quad [\mathbf{G}^*] = \int_0^l [\mathbf{N}_{\beta\gamma}]^t I_P [\mathbf{N}_{\beta\beta}]\, \mathrm{d}x, \quad C^* = \int_0^l I_P\, \mathrm{d}x,$$

$$[\mathbf{M}_e] = \int_0^l I_P([\mathbf{N}_\phi]^t[\mathbf{N}_{\beta\gamma}]\{\mathbf{e}\}[\mathbf{N}_{\beta\beta}] - [\mathbf{N}_\phi]^t[\mathbf{N}_{\beta\beta}]\{\mathbf{e}\}[\mathbf{N}_{\beta\gamma}])\, \mathrm{d}x,$$

where $A(x)$ is the cross-sectional area, $l$ is the length, $I_D$ is the diametral mass moment of inertia, and $I_P$ is the polar mass moment of inertia of the shaft element. The matrix

$$[\mathbf{N}_\beta] = \begin{bmatrix} \mathbf{N}_{\beta\beta} \\ \mathbf{N}_{\beta\gamma} \end{bmatrix}$$

represents rotational shape functions and $[\mathbf{N}_\phi]$ of torsional shape functions. The shape functions and the non-zero elements of the time dependent matrix $[\mathbf{M}_e]$ are given in the Appendix.

### 2.3. STRAIN ENERGY OF THE SHAFT

Neglecting axial deformation, the potential energy of the shaft element can be written as

$$U = \frac{1}{2}\int_0^l EI\left\{\left(\frac{\partial\beta}{\partial x}\right)^2 + \left(\frac{\partial\gamma}{\partial x}\right)^2\right\}\mathrm{d}x + \frac{1}{2}\int_0^l \kappa GA\left\{\left(\frac{\partial v}{\partial x} - \gamma\right)^2 + \left(\frac{\partial w}{\partial x} + \beta\right)^2\right\}\mathrm{d}x$$
$$+ \frac{1}{2}\int_0^l GJ\left(\frac{\partial\phi}{\partial x}\right)^2 \mathrm{d}x, \tag{6}$$

where $v$ and $w$ are flexural deformations in $Y$ and $Z$-directions, while $\phi$, $\beta$ and $\gamma$ are small rotations about the $X$-, $j_2$- and $k$-axes, respectively, $E$ is the modulus of elasticity, $G$ is the shear modulus of the shaft material, $I$ is the second moment of cross-sectional area, $J$ is the polar moment of inertia and $\kappa$ is the shear correction factor. Equation (6) can be written in matrix form as

$$U = \frac{1}{2}\{\mathbf{e}\}^t[\mathbf{K}]\{\mathbf{e}\}. \tag{7}$$

The matrix [**K**] is the composite element stiffness matrix given by

$$[\mathbf{K}] = [\mathbf{K}_e] + [\mathbf{K}_s] + [\mathbf{K}_\phi],$$

where $[\mathbf{K}_e]$ is the elastic stiffness matrix, $[\mathbf{K}_s]$ is the shear stiffness matrix and $[\mathbf{K}_\phi]$ is the torsional stiffness matrix. These are defined as

$$[\mathbf{K}_e] = \int_0^l \left(\frac{\partial}{\partial x}[\mathbf{N}_\beta]\right)^t EI\left(\frac{\partial}{\partial x}[\mathbf{N}_\beta]\right) \mathrm{d}x, \quad [\mathbf{K}_\phi] = \int_0^l \left(\frac{\partial}{\partial x}[\mathbf{N}_\phi]\right)^t GJ\left(\frac{\partial}{\partial x}[\mathbf{N}_\phi]\right) \mathrm{d}x,$$

$$[\mathbf{K}_s] = \int_0^l \kappa GA \begin{bmatrix} \dfrac{\partial}{\partial x}[\mathbf{N}_{vv}] - [\mathbf{N}_{\beta\gamma}] \\ \dfrac{\partial}{\partial x}[\mathbf{N}_{vw}] + [\mathbf{N}_{\beta\beta}] \end{bmatrix}^t \begin{bmatrix} \dfrac{\partial}{\partial x}[\mathbf{N}_{vv}] - [\mathbf{N}_{\beta\gamma}] \\ \dfrac{\partial}{\partial x}[\mathbf{N}_{vw}] + [\mathbf{N}_{\beta\beta}] \end{bmatrix} \mathrm{d}x.$$

Here, the different shape functions are defined by the following relationships:

$$\begin{Bmatrix} v \\ w \end{Bmatrix} = [\mathbf{N}_v]\{\mathbf{e}\} = \begin{bmatrix} [\mathbf{N}_{vv}] \\ [\mathbf{N}_{vw}] \end{bmatrix}\{\mathbf{e}\},$$

$$\begin{Bmatrix} \beta \\ \gamma \end{Bmatrix} = [\mathbf{N}_\beta]\{\mathbf{e}\} = \begin{bmatrix} [\mathbf{N}_{\beta\beta}] \\ [\mathbf{N}_{\beta\gamma}] \end{bmatrix}\{\mathbf{e}\},$$

$$\{\phi\} = [\mathbf{N}_\phi]\{\mathbf{e}\}.$$

### 2.4. THE ROTOR-BEARING SYSTEM

The rotor-bearing system consists of a rotating shaft, disks and bearings. The rotating shaft is divided into number of finite elements. The bearings can be flexible and damped. Isotropic as well as anisotropic bearings can be accommodated. The disks are considered to be rigid. Now the equation of motion of each part of the rotor-bearing system will be derived separately.

#### 2.4.1. *Equation of motion of the shaft element*

Using the Lagrangian approach, the equation of motion can be derived as

$$[\mathbf{M}]\{\ddot{\mathbf{e}}\} + \dot{\theta}[\mathbf{G}]\{\dot{\mathbf{e}}\} + [\mathbf{K}]\{\mathbf{e}\} = \{\mathbf{Q}\}, \tag{8}$$

where [**M**] is the composite element mass matrix, $[\mathbf{G}] = [\mathbf{G}^*] - [\mathbf{G}^*]^t$ is the element

gyroscopic matrix, [**K**] is the composite element stiffness matrix and {**Q**} is a vector of generalized forces.

2.4.2. *The disk*

The equation of motion of the rigid disk is derived as

$$[\mathbf{M}^d]\{\ddot{\mathbf{e}}\} + \dot{\theta}[\mathbf{G}^d]\{\dot{\mathbf{e}}\} = \{\mathbf{Q}^d\}, \tag{9}$$

where $[\mathbf{M}^d]$ is the disk mass matrix, $[\mathbf{G}^d]$ is the gyroscopic matrix and $\{\mathbf{Q}^d\}$ is the vector of generalized forces of the disk.

2.4.3. *The bearings*

The generalized forces acting on the bearings can be written as

$$[\mathbf{C}^b]\{\dot{\mathbf{e}}\} + [\mathbf{K}^b]\{\mathbf{e}\} = \{\mathbf{Q}^b\}, \tag{10}$$

where $[\mathbf{C}^b]$ is the bearing damping matrix, $[\mathbf{K}^b]$ is the bearing stiffness matrix and $\{\mathbf{Q}^b\}$ is the vector of generalized forces of the bearings.

Now, the equation of motion of a rotor-bearing system can be written in the assembled general form as

$$[\bar{\mathbf{M}}]\{\ddot{\bar{\mathbf{e}}}\} + [\bar{\mathbf{C}}]\{\dot{\bar{\mathbf{e}}}\} + [\bar{\mathbf{K}}]\{\bar{\mathbf{e}}\} = \{\bar{\mathbf{Q}}\}, \tag{11}$$

where $[\bar{\mathbf{M}}]$ is the assembled mass matrix of the system taking into account the disk mass matrix at the corresponding locations. Similarly $[\bar{\mathbf{C}}]$ is the assembled gyroscopic matrix, $[\bar{\mathbf{K}}]$ is the assembled stiffness matrix and $\{\bar{\mathbf{Q}}\}$ is the assembled generalized force vector. The vector $\{\bar{\mathbf{e}}\}$ is the assembled vector of nodal co-ordinates of the whole system.

## 3. MODAL TRUNCATION OF THE ELASTODYNAMIC EQUATIONS

The elastodynamic model of equation (11) can be represented in the state–space form as

$$\begin{bmatrix} \mathbf{0} & -\bar{\mathbf{M}} \\ \bar{\mathbf{M}} & \bar{\mathbf{C}} \end{bmatrix} \begin{Bmatrix} \ddot{\bar{\mathbf{e}}} \\ \dot{\bar{\mathbf{e}}} \end{Bmatrix} + \begin{bmatrix} \bar{\mathbf{M}} & \mathbf{0} \\ \mathbf{0} & \bar{\mathbf{K}} \end{bmatrix} \begin{Bmatrix} \dot{\bar{\mathbf{e}}} \\ \bar{\mathbf{e}} \end{Bmatrix} = \begin{Bmatrix} \mathbf{0} \\ \bar{\mathbf{Q}} \end{Bmatrix}. \tag{12}$$

Or simply as

$$[\mathbf{A}]\{\dot{\mathbf{q}}\} + [\mathbf{B}]\{\mathbf{q}\} = \{\mathbf{f}\}, \tag{13}$$

where $\{\mathbf{q}\} = \{\{\dot{\bar{\mathbf{e}}}\}^t, \{\bar{\mathbf{e}}\}^t\}^t$. One can write the following two homogeneous adjoint equations

$$[\mathbf{A}]\{\dot{\mathbf{q}}\} + [\mathbf{B}]\{\mathbf{q}\} = \{\mathbf{0}\} \quad \text{and} \quad [\mathbf{A}]^t\{\dot{\mathbf{q}}\}^t + [\mathbf{B}]^t\{\mathbf{q}\}^t = \{\mathbf{0}\}. \tag{14, 15}$$

Let [**R**] and [**L**] denote the complex modal matrices of the differential operators of equations (14) and (15), respectively [20]. Introducing the transformation

$$\{\mathbf{q}\} = [\mathbf{R}]\{\mathbf{u}\}, \tag{16}$$

where $\{\mathbf{u}\}$ is the vector of modal co-ordinates. If only a subset of significant

modes are to be retained, the truncated modal form of the equations of motion can be written as

$$[\mathbf{L}]^t[\mathbf{A}][\mathbf{R}]\{\dot{\mathbf{u}}\} + [\mathbf{L}]^t[\mathbf{B}][\mathbf{R}]\{\mathbf{u}\} = [\mathbf{L}]^t\{\mathbf{f}\}, \tag{17}$$

Or, simply as

$$[\bar{\mathbf{A}}]\{\dot{\mathbf{u}}\} + [\bar{\mathbf{B}}]\{\mathbf{u}\} = [\mathbf{L}]^t\{\mathbf{f}\}, \tag{18}$$

where [**R**] and [**L**] contain only those complex eigenvectors that represent a subset of selected modes.

In the modal transformation of equation (18), the eigenvectors were used with their full length. However, similar modal transformations can be established using a subset of eigenvectors with truncated length [19]. In this regard, the modal co-ordinate vector {**q**} can be partitioned as

$$\{\mathbf{q}\} = \begin{Bmatrix} \mathbf{q}_r \\ \mathbf{q}_o \end{Bmatrix} = \begin{bmatrix} \mathbf{R}_r \\ \mathbf{R}_o \end{bmatrix}\{\mathbf{u}\}, \tag{19}$$

where $\{\mathbf{q}_r\}$ is the retained subset of nodal co-ordinates, and $\{\mathbf{q}_o\}$ is the omitted subset of nodal co-ordinates. The modal co-ordinate vector can be expressed in terms of the retained subset of nodal co-ordinates as

$$\{\mathbf{u}\} = ([\mathbf{R}_r]^t[\mathbf{R}_r])^{-1}[\mathbf{R}_r]^t\{\mathbf{q}_r\}. \tag{20}$$

Utilizing equations (19) and (20) one can write

$$\{\mathbf{q}_o\} = [\mathbf{R}_o]([\mathbf{R}_r]^t[\mathbf{R}_r])^{-1}[\mathbf{R}_r]^t\{\mathbf{q}_r\} = [\mathbf{Q}_R]\{\mathbf{q}_r\}. \tag{21}$$

Similarly, for the left-hand modal transformation [**L**], one gets

$$\{\mathbf{q}_o\} = [\mathbf{L}_o]([\mathbf{L}_r]^t[\mathbf{L}_r])^{-1}[\mathbf{L}_r]^t\{\mathbf{q}_r\} = [\mathbf{Q}_L]\{\mathbf{q}_r\}. \tag{22}$$

Now, the following relations can be established:

$$\{\mathbf{R}\} = [\mathbf{H}_R]\{\mathbf{R}_r\}, \quad \{\mathbf{L}\} = [\mathbf{H}_L]\{\mathbf{L}_r\}, \tag{23, 24}$$

where

$$[\mathbf{H}_R] = \begin{bmatrix} \mathbf{I} \\ \mathbf{G}_R \end{bmatrix}, \quad [\mathbf{H}_L] = \begin{bmatrix} \mathbf{I} \\ \mathbf{G}_L \end{bmatrix}.$$

Substituting equations (23) and (24) into equation (17) one gets,

$$[\mathbf{L}_r]^t[\mathbf{H}_L]^t[\mathbf{A}][\mathbf{H}_R][\mathbf{R}_r]\{\dot{\mathbf{u}}\} + [\mathbf{L}_r]^t[\mathbf{H}_L]^t[\mathbf{B}][\mathbf{H}_R][\mathbf{R}_r]\{\mathbf{u}\} = [\mathbf{L}_r]^t\{\mathbf{f}\} \tag{25}$$

or

$$[\mathbf{L}_r]^t[\mathbf{A}_r][\mathbf{R}_r]\{\dot{\mathbf{u}}\} + [\mathbf{L}_r]^t[\mathbf{B}_r][\mathbf{R}_r]\{\mathbf{u}\} = [\mathbf{L}_r]^t\{\mathbf{f}\}, \tag{26}$$

where the reduced matrices $[\mathbf{A}_r]$ and $[\mathbf{B}_r]$ are those used by Kane and Torby [19]

to evaluate the modal characteristics of a rotating shaft. Equation (26) can be written as

$$[\bar{\mathbf{A}}_r]\{\dot{\mathbf{u}}\} + [\bar{\mathbf{B}}_r]\{\mathbf{u}\} = [\mathbf{L}]^t\{\mathbf{f}\}. \tag{27}$$

It is worth noting that the self adjoint operator associated with the reduced diagonal matrices $[\bar{\mathbf{A}}]$ and $[\bar{\mathbf{B}}]$ of equation (7) or $[\bar{\mathbf{A}}_r]$ and $[\bar{\mathbf{B}}_r]$ of equation (27) or the reduced nondiagonal matrices $[\mathbf{A}_r]$ and $[\mathbf{B}_r]$ of equation (26) have the same eigenvalues as those produced by the original full size matrices [**A**] and [**B**] of equation (13). Now, for dynamic response solutions, one can use either the reduced model of equation (18) or the reduced model of equation (27). However equation (27) may be preferred for experimentally determined modal data of large scale problems.

## 4. RESULTS AND DISCUSSION

Three numerical examples are simulated to study the dynamic response of different rotor systems. As a first example, a uniform steel shaft rotating at 400 rad/s and supported at the two ends by rigid bearings (simply supported) is considered. The shaft is of diameter $d = 10{\cdot}16$ cm and length $l = 127$ cm. The density and elastic modulus of the shaft material are $\rho = 0{\cdot}7833 \times 10^4$ kg/m$^3$ and $E = 0{\cdot}2068 \times 10^{12}$ N/m$^2$, respectively. This particular example is selected to validate the results from the dynamic analysis code developed during this study by comparing with the results from an established commercially available finite element software ANSYS. The rotating shaft is divided into six equal finite elements and is excited by a unit step force in the $Y$ direction at the midpoint of the shaft. The response of the system is computed using both the programs. Figure 3 gives a comparison of the deflection in the $Y$ direction of the midpoint of the rotating shaft, when the response is computed using (a) $(62 \times 62)$ full dimension state space matrices with the currently developed code, (b) $(4 \times 4)$ reduced dimension state space matrices with the currently developed code, and (c) using full dimension matrices with ANSYS software. The response of the shaft using the dynamic analysis code developed during this study is agreeable with the response computed using ANSYS software. Hence, the developed dynamic analysis code using the complex modal reduction technique is validated.

As a second example, the rotating shaft studied in the first example with the same geometry, rotating speed and material constants is used, but is supported at the two ends by flexible damped bearings (Figure 4). The stiffness coefficients of the bearings are $K_{yy} = K_{zz} = 1{\cdot}7513 \times 10^7$ N/m, $K_{yz} = K_{zy} = -2{\cdot}917 \times 10^6$ N/m and the damping coefficients are $C_{yy} = C_{zz} = 1{\cdot}752 \times 10^3$ N s/m and $C_{yz} = C_{zy} = 0{\cdot}0$. The shaft is divided into six equal finite elements. The modal characteristics of the rotor bearing system are generated utilizing the full-dimension matrices [**A**], [**B**] of equation (13), and compared to those of reference [21] in Table 1. For the purpose of this comparison, the shaft has been divided into five equal finite beam elements.

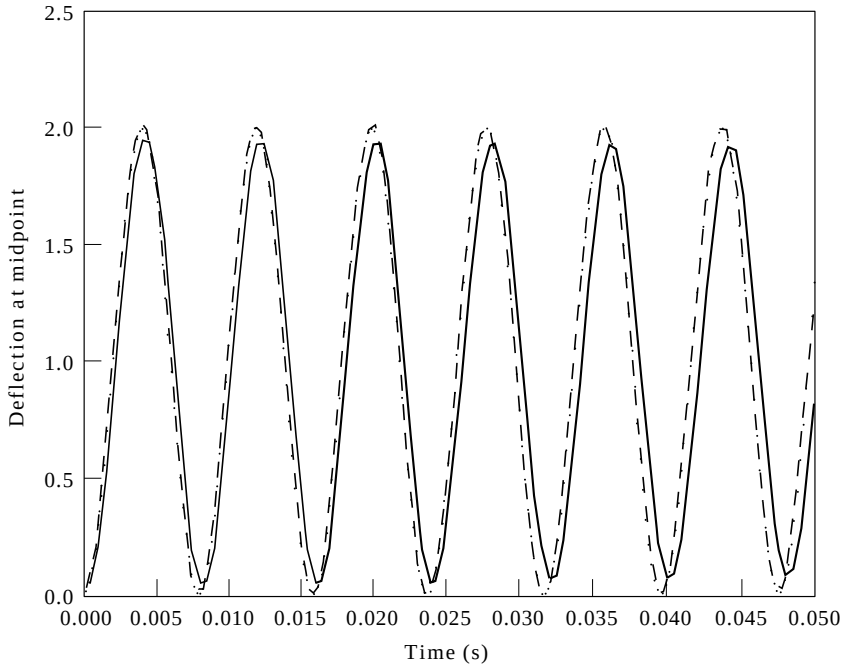


Figure 3. Comparison of time response. —, ANSYS; – – –, full order; · · · · · ·, reduced order.

The modal characteristics are then reproduced using the reduced-order modal matrices $[\bar{\mathbf{A}}]$, $[\bar{\mathbf{B}}]$ of equation (18) and $[\mathbf{A}_r]$, $[\mathbf{B}_r]$ of equation (26), respectively, to show their validity in preserving the significant modes of the original system. In this case, the shaft has been modeled by six finite elements, and modal transformations were established to preserve the lower dynamics of the first forward and backward flexural modes, as well as the first torsional mode. Therefore, the $(70 \times 70)$ full dimension state space matrices have been reduced to $(5 \times 5)$ modal matrices, as tabulated in Table 2. The eigenvalue solutions of the full-dimension and the reduced-dimension matrices are presented in Table 3.

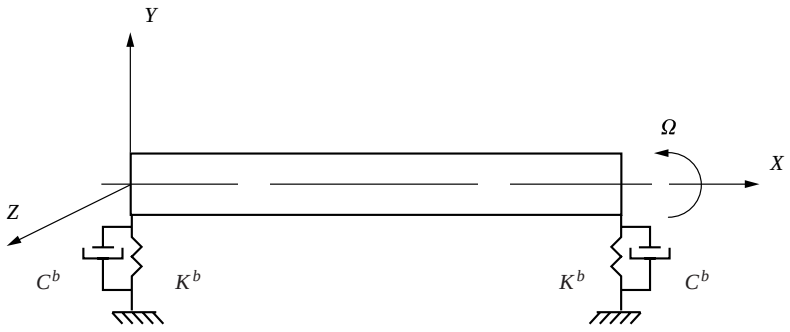


Figure 4. A rotating shaft supported by flexible bearings.

TABLE 1

*Damped frequencies of the rotor system of example 2*

| | Reference [21] | | Present work | |
|---|---|---|---|---|
| Mode | $\omega_d$ (rad/s) | $\delta$ | $\omega_d$ (rad/s) | $\delta$ |
| 1B | 491·90 | 0·1208 | 490·91 | 0·1200 |
| 1F | 544·79 | 0·0826 | 543·48 | 0·0819 |
| 2B | 1005·0 | 0·3553 | 1003·71 | 0·3538 |
| 2F | 1174·2 | 0·2879 | 1172·04 | 0·2862 |
| 3B | 2171·7 | 0·2715 | 2161·16 | 0·2715 |
| 3F | 2312·7 | 0·2571 | 2301·99 | 0·2567 |
| 4B | 5038·7 | 0·1122 | 4944·85 | 0·1143 |
| 4F | 5107·4 | 0·1134 | 5013·39 | 0·1156 |
| 5B | – | – | 9250·56 | 0·0586 |
| 5F | – | – | 9308·74 | 0·059 |

To demonstrate the capability of the developed model, the time-response of the rotor due to a unit force in the $Y$ direction, appled at the midpoint of the shaft, is computed. In this simulation, the time response is expressed as a non-dimensional generalized displacement parameter $\eta$ plotted against time. For

TABLE 2

*The reduced matrices*

(a) The reduced matrices of equation (18):

$$[\bar{\mathbf{A}}] = \mathrm{diag}\begin{bmatrix} -6{\cdot}981 - 10{\cdot}436\mathrm{i}, \\ -6{\cdot}981 + 10{\cdot}436\mathrm{i}, \\ -3{\cdot}793 + 9{\cdot}22\mathrm{i}, \\ 9{\cdot}918 - 1{\cdot}017\mathrm{i}, \\ 0{\cdot}024 - 0{\cdot}0065\mathrm{i} \end{bmatrix}, \quad [\bar{\mathbf{B}}] = \mathrm{diag}\begin{bmatrix} 0{\cdot}215 - 0{\cdot}0138\mathrm{i}, \\ 0{\cdot}0226 + 0{\cdot}012\mathrm{i}, \\ -0{\cdot}0168 - 0{\cdot}0072\mathrm{i}, \\ -0{\cdot}0021 - 0{\cdot}0182\mathrm{i}, \\ -8{\cdot}25 \end{bmatrix}$$

(b) The reduced matrices of equation (26):

$$[\mathbf{A}_r] = \begin{bmatrix} -75\,184{\cdot}03 & 33\,676{\cdot}71 & 8966{\cdot}15 & 30\,379{\cdot}51 & 0 \\ 19\,804{\cdot}16 & -75\,183{\cdot}01 & -31\,440{\cdot}59 & -2899{\cdot}01 & 0 \\ 2898{\cdot}65 & -30\,379{\cdot}39 & -13\,057{\cdot}27 & 1058{\cdot}15 & 0 \\ 31\,439{\cdot}97 & -8964{\cdot}90 & -1513{\cdot}79 & -13\,056{\cdot}92 & 0 \\ 0 & 0 & 0 & 0 & 1{\cdot}65 \times 10^{-6} \end{bmatrix}$$

$$[\mathbf{B}_r] = \begin{bmatrix} 13{\cdot}45 & -2{\cdot}80 & 0{\cdot}08 & -2{\cdot}51 & 0 \\ -0{\cdot}68 & 13{\cdot}45 & 2{\cdot}50 & -0{\cdot}65 & 0 \\ 0{\cdot}65 & 2{\cdot}51 & -0{\cdot}29 & -0{\cdot}19 & 0 \\ -2{\cdot}50 & -0{\cdot}08 & -0{\cdot}09 & -0{\cdot}29 & 0 \\ 0 & 0 & 0 & 0 & 0 \end{bmatrix}$$

TABLE 3
*The comparison of eigenvalues of the rotor system of example* 2

| No | Eigenvalues | | |
|---|---|---|---|
| | Using matrices of equation (13) | Using matrices of equation (18) | Using matrices of equation (26) |
| 1 | $-9{\cdot}38 \pm 490{\cdot}86$i† | $-9{\cdot}38 \pm 490{\cdot}86$i | $-9{\cdot}38 \pm 490{\cdot}86$i |
| 2 | $-7{\cdot}08 \pm 543{\cdot}37$i† | $-7{\cdot}08 \pm 543{\cdot}37$i | $-7{\cdot}08 \pm 543{\cdot}37$i |
| 3 | $-56{\cdot}47 \pm 1003{\cdot}44$i | $0 + 7840{\cdot}80$i | $0 + 7840{\cdot}80$i |
| 4 | $-53{\cdot}33 \pm 1171{\cdot}68$i | | |
| 5 | $-93{\cdot}12 \pm 2159{\cdot}19$i | | |
| 6 | $-93{\cdot}73 \pm 2300{\cdot}10$i | | |
| 7 | $-88{\cdot}99 \pm 4930{\cdot}76$i | | |
| 8 | $-91{\cdot}18 \pm 4998{\cdot}76$i | | |
| 9 | $0 \pm 7840{\cdot}80$i†‡ | | |

† Selected in reduced order equation.
‡ First torsional natural frequency.

transverse deflections in the $Y$ and $Z$ directions, the non-dimensional generalized displacement parameters are defined as

$$\eta_y = \frac{v}{\Delta} \quad \text{and} \quad \eta_z = \frac{w}{\Delta}, \tag{28}$$

where $v$ is the deflection in the $Y$ direction, $w$ is the deflection in the $Z$ direction

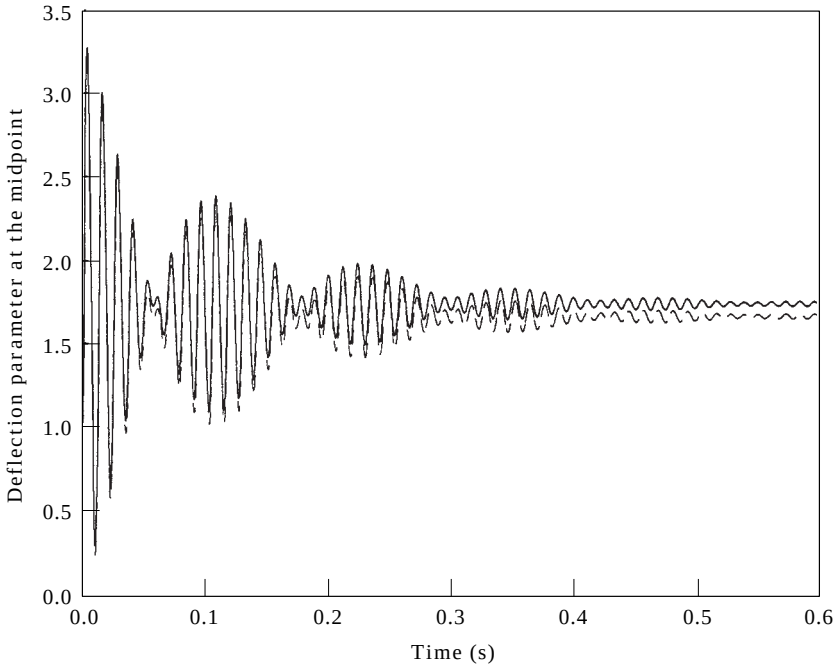


Figure 5. Deflection due to step force in the $Y$ direction at the midpoint of the shaft. —, Full order model; – – –, 5th order reduced model.

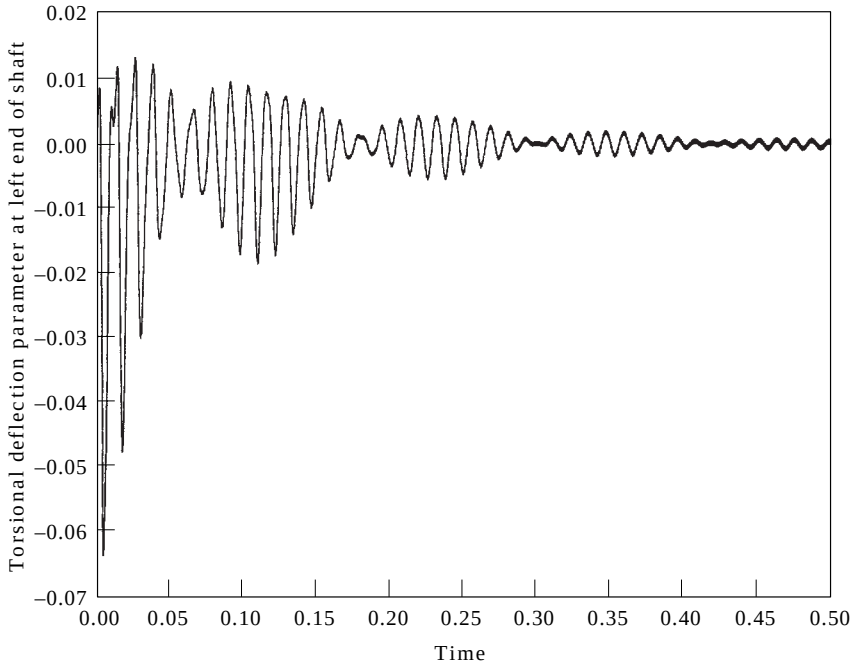


Figure 6. Deflection due to step force in the $Y$ direction at the midpoint of the shaft.

and $\Delta$ is the static deflection at the point of application of force in the direction of the force. For the torsional deflection the non-dimensional generalized displacement parameter is defined as

$$\eta_\phi = \frac{\phi}{2\Delta/d}, \tag{29}$$

where $\phi$ is the torsional deformation and $d$ is the diameter of the shaft at the point of measurement. The transverse and torsional time-responses of the midpoint are shown, respectively, in Figures 5 and 6. In Figure 5, the response

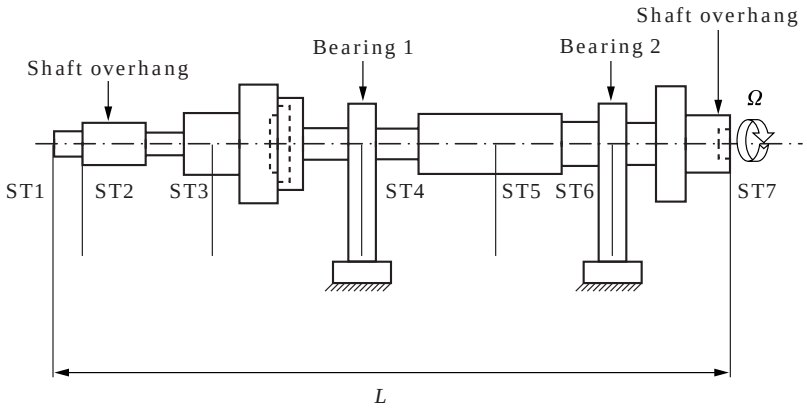


Figure 7. Configuration of multi-stepped rotor-bearing system.

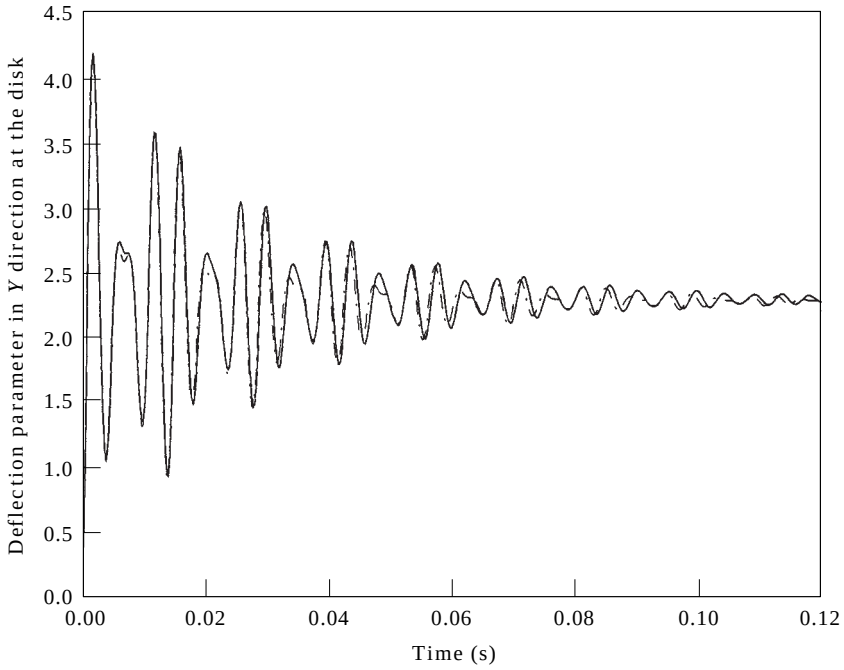


Figure 8. Deflection due to step force in the $Y$ direction at the disk. —, Full order model; – – –, 5th order reduced model.

of the full order model is compared to the response of the reduced model of order of five, which shows good agreement with the full order model. It is worth mentioning that the torsional vibrations shown in Figure 6 are induced mainly by the inertia coupling between flexural and torsional vibrations. Since there is no damping on either the torsional or rotational motions, the torsional vibrations, unlike flexural vibrations, will not die away.

As a third example, the rotor-bearing system studied by Nelson and McVaugh [4] is used to illustrate the merits of the present mathematical formulation for the determination of natural frequencies and time responses. The configuration of the rotor system is shown in Figure 7 and the corresponding data are given in reference [21]. The rotor-bearing system is rotating at a constant speed of $\Omega = 2000$ rad/s. The reduced matrices are obtained by selecting the corresponding modes of the first transverse backward and forward frequencies and the first torsional frequency, thus replacing the $(190 \times 190)$ full-dimension matrices by reduced ones of order $(5 \times 5)$. The rotor system is excited by a unit force acting in the $Y$ direction on the disk which is located at the fifth node. The deflection in the $Y$ direction at the disk location is shown in Figure 8, while the deflection in the $Z$ direction at the disk due to the same unit force in the $Y$ direction is shown in Figure 9. The deflections obtained from the full order model are compared to the deflection obtained from the reduced model of order five and found to be in good agreement. The deflection in the $Z$ direction due to the unit force in the $Y$ direction is induced because of the coupling between flexural deformations in the $Y$ and $Z$ directions. It can be noted that the points

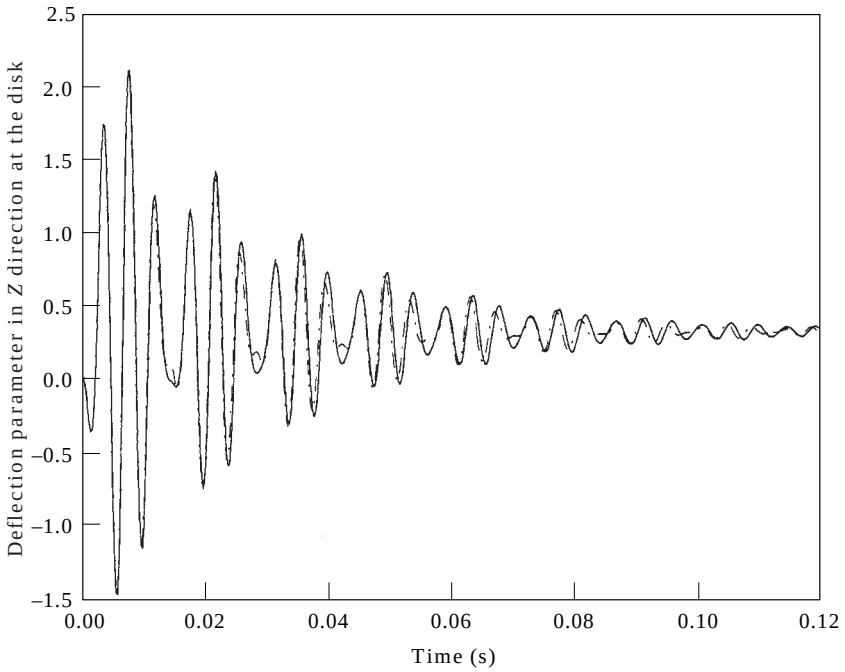


Figure 9. Deflection due to step force in the $Y$ direction at the disk. —, Full order model; – – –, 5th order reduced model.

of small deflections in the $Y$ direction correspond, in general, to the points of large deflections in the $Z$ direction and vice-versa. In Figure 10, the torsional deflection at ST1 due to the unit force in the $Y$ direction is shown. This torsional deflection is due to the inertia coupling of the flexural and torsional vibrations. In this simulation, the amplitude of the torsional deflection does not diminish to zero because no damping is provided for the torsional motion of the rotor-bearing system. The numerical examples presented here demonstrate the capability of the solution scheme developed in simulating the rotor's time response due to a general forcing function. The developed scheme may, therefore, be utilized in studying time response due to shock loading conditions as well as any type of lateral or torsional control forces.

## 5. CONCLUSIONS

A finite element elastodynamic model of a rotor-bearing system is formulated. The model accounts for the gyroscopic effects, as well as the coupling between flexural and torsional deformations. In addition, the formulation permits the use of either a uniform or tapered shaft element, and a general anisotropic bearing. The finite element model accounts for rotary inertia and shear deformations. The full dimension equations of motion of the original system have been reduced by invoking a modal transformation that utilizes the complex mode shapes of the rotor system. The reduced order state space matrices are shown to preserve the selected significant modes of the original system. In addition, the reduced order

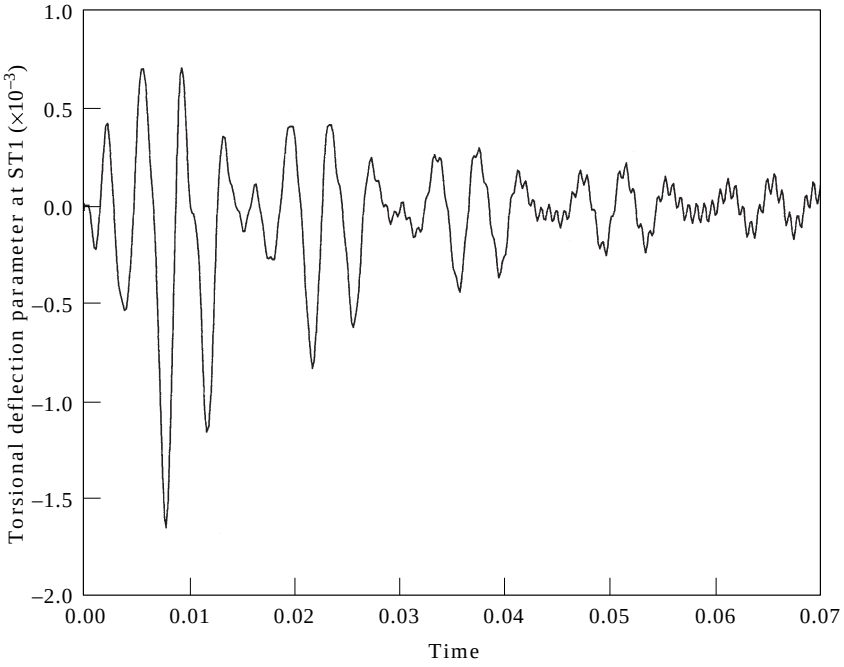


Figure 10. Deflection due to step force in the $Y$ direction at the disk.

modal form of the equations of motion is integrated forward in time to study the dynamic behavior of the system. The efficiency of the reduced order model is manifested by preserving the lower or the significant modes of the original system while accounting for the inertia coupling effects. Therefore, the developed model provides an efficient tool for dynamic analysis of rotor-bearing systems, and validates the use of reduced order modal equations for complex rotor systems.

## ACKNOWLEDGMENT

The authors appreciate the support provided by the King Fahd University of Petroleum & Minerals during this research.

## REFERENCES

1. F. Dimentberg 1961 *Flexural Vibrations of Rotating Shafts*. London: Butterworth.
2. H. Black 1974 *Journal of Engineering for Industry*. A linearized model using transfer matrix to study the forced whirling of centrifugal pumps rotor systems.
3. R. L. Ruhl and J. F. Booker 1972 *ASME Journal of Engineering for Industry* **94**, 126–132. A finite element model for distributed parameter turborotor systems.
4. H. D. Nelson and J. M. McVaugh 1976 *ASME Journal of Engineering for Industry* **98**, 593–600. The dynamics of rotor-bearing systems using finite element.
5. E. S. Zorzi and H. D. Nelson 1980 *Journal of Mechanical Engineering Design* **102**, 158–161. The dynamics of rotor-bearing systems with axial torque—a finite element approach.

6. H. D. NELSON 1980 *Journal of Mechanical Design* **102**, 793–803. A finite rotating shaft element using Timoshenko beam theory.
7. L.-W. CHEN and D.-M. KU 1991 *Computers and Structures* **40**, 741–747. Finite element analysis of natural whirl speeds of rotating shafts.
8. K. E. ROUCH and J. S. KAO 1979 *Journal of Sound and Vibration* **66**, 119–140. A tapered beam finite element for rotor dynamic analysis.
9. L. M. GREENHILL, W. B. BICKFORD and H. D. NELSON 1985 *ASME Journal of Vibration and Acoustics* **107**, 421–430. A conical beam finite element for rotor dynamic analysis.
10. T. C. GMUR and J. D. RODRIGUES 1991 *Journal of Vibration and Acoustics* **113**, 482–493. Shaft finite elements for rotor dynamic analysis.
11. M. A. MOHIUDDIN and Y. A. KHULIEF 1994 *Computer Methods in Applied Mechanics and Engineering* **115**, 125–144. Modal characteristics of rotors using a conical shaft finite element.
12. R. FIROOZIAN and R. STANWAY 1988 *Journal of Vibration and Acoustics, Stress, and Reliability in Design* **110**, 521–527. Modeling and control of turbomachinery vibrations.
13. W. DIEWALD and R. NORDMANN 1989 *ASME Journal of Vibration and Acoustics, Stress, and Reliability in Design* **111**, 370–378. Dynamic analysis of centrifugal pump rotors with fluid–mechanical interactions.
14. M. SAKATA, K. KIMURA, S. K. PARK and H. OHNABE 1989 *Journal of Sound and Vibration* **131**, 417–430. Vibration of bladed flexible rotor due to gyroscopic moments.
15. K. E. ROUCH, T. H. MCMAINES, R. W. STEPHENSON and M. F. ERMERICK 1989 4*th International ANSYS Conference and Exhibition, Part* 2, 5.23–5.39. Modeling of complex rotor systems by combining rotor and substructure models.
16. P. W. LIKINS 1972 *International Journal of Solids and Structures* **8**, 709–731. Finite element appendage equations for hybrid coordinate dynamic analysis.
17. A. A. SHABANA and WEHAGE 1983 *ASME Journal of Mechanical Transactions and Automation in Design* **105**, 370–378. Variable degree of freedom compact mode analysis of inertia variant flexible machine systems.
18. Y. A. KHULIEF 1992 *Computer Methods in Applied Mechanics and Engineering* **97**, 23–32. On the finite element dynamic analysis of flexible mechanisms.
19. K. KANE and B. J. TORBY 1991 *ASME Journal of Vibration and Acoustics* **113**, 79–84. The extended modal reduction method applied to rotor dynamic problems.
20. J. H. WILKINSON 1965 *The Algebraic Eigenvalue Problem* Oxford: Clarendon Press.
21. T. N. SHIAU and J. L. HWANG 1991 *The* 36*th ASME International Gas Turbine and Aeroengine Congress and Exposition, Orlando, FL*. Generalized polynomial expansion method for the dynamic analysis of rotor-bearing system.

## APPENDIX

The nodal co-ordinate vector $\{\mathbf{e}\}$ is given by

$$\{\mathbf{e}\} = \{v_i, w_i, \beta_i, \gamma_i, \phi_i, v_j, w_j, \beta_j, \gamma_j, \phi_j\}^t, \tag{A1}$$

where $v$ and $w$ are the transverse deformations in the $Y$ and $Z$ directions, $\beta$, $\gamma$ and $\phi$ are rotational deformations about $Y$, $Z$, and $X$, respectively. The subscript $i$ represents the left node of the shaft element and $j$ represents the right node of the shaft element.

The translation of a point internal to the element can be aproximated by

$$\begin{Bmatrix} v(x,t) \\ w(x,t) \end{Bmatrix} = [\mathbf{N}_v(x)]\{\mathbf{e}(t)\} = \begin{bmatrix} \mathbf{N}_{vv}(x) \\ \mathbf{N}_{vw}(x) \end{bmatrix}\{\mathbf{e}(t)\}$$
$$= \begin{bmatrix} N_{v_1} & 0 & 0 & N_{v_2} & 0 & N_{v_3} & 0 & 0 & N_{v_4} & 0 \\ 0 & N_{v_1} & -N_{v_2} & 0 & 0 & 0 & N_{v_3} & -N_{v_4} & 0 & 0 \end{bmatrix}\{\mathbf{e}(t)\}. \tag{A2}$$

The rotation of a typical cross-section of the element is approximated by

$$\begin{Bmatrix} \beta(x,t) \\ \gamma(x,t) \end{Bmatrix} = [\mathbf{N}_\beta(x)]\{\mathbf{e}(t)\} = \begin{bmatrix} \mathbf{N}_{\beta\beta}(x) \\ \mathbf{N}_{\beta\gamma}(x) \end{bmatrix}\{\mathbf{e}(t)\}$$
$$= \begin{bmatrix} 0 & -N_{\beta_1} & N_{\beta_2} & 0 & 0 & 0 & -N_{\beta_3} & N_{B_4} & 0 & 0 \\ N_{\beta_1} & 0 & 0 & N_{\beta_2} & 0 & N_{\beta_3} & 0 & 0 & N_{\beta_4} & 0 \end{bmatrix}\{\mathbf{e}(t)\}. \tag{A3}$$

The torsional deflection of a typical cross-section of the element is approximated by

$$\phi(x,t) = [\mathbf{N}_\phi(x)]\{\mathbf{e}(t)\} = [0 \quad 0 \quad 0 \quad 0 \quad N_{\phi_1} \quad 0 \quad 0 \quad 0 \quad 0 \quad N_{\phi_2}]\{\mathbf{e}(t)\}. \tag{A4}$$

The individual shape functions are as follows:

$$N_{v_1} = \frac{1}{1+\Phi}[1 - 3\xi^2 + 2\xi^3 + \Phi(1-\xi)], \tag{A5}$$

$$N_{v_2} = \frac{l}{1+\Phi}\left[\xi - 2\xi^2 + \xi^3 + \frac{\Phi}{2}(\xi - \xi^2)\right], \tag{A6}$$

$$N_{v_3} = \frac{1}{1+\Phi}[3\xi^2 - 2\xi^3 + \Phi\xi], \tag{A7}$$

$$N_{v_4} = \frac{l}{1+\Phi}\left[-\xi^2 + \xi^3 + \frac{\Phi}{2}(-\xi + \xi^2)\right], \tag{A8}$$

$$N_{\beta_1} = \frac{6}{l(1+\Phi)}[\xi^2 - \xi], \tag{A9}$$

$$N_{\beta_2} = \frac{1}{1+\Phi}[1 - 4\xi + 3\xi^2 + \Phi(1-\xi)], \tag{A10}$$

$$N_{\beta_3} = \frac{6}{l(1+\Phi)}[\xi - \xi^2], \tag{A11}$$

$$N_{\beta_4} = \frac{1}{1+\Phi}[-2\xi + 3\xi^2 + \Phi\xi], \tag{A12}$$

$$N_{\phi_1} = 1 - \xi, \tag{A13}$$

$$N_{\phi_2} = \xi. \tag{A14}$$

The transverse shear effect is $\Phi = (12EI)/(\kappa AGl^2)$ and $\xi = x/l$.

The non-zero elements of the time dependent matrix $[\mathbf{M}_e]$ are as follows:

$$(M_e)_{5,1} = \frac{I_i}{420l^2(1+\Phi)^2}\{6w_j p_{at1} - l\beta_i p_{at2} - l\beta_j p_{at3} - 6w_i p_{at1}\}, \tag{A15}$$

$$(M_e)_{5,2} = \frac{-I_i}{420l^2(1+\Phi)^2}\{6v_j p_{at1} + l\gamma_i p_{at2} - l\gamma_j p_{at3} - 6v_i p_{at1}\}, \tag{A16}$$

$$(M_e)_{5,3} = \frac{I_i}{840l^2(1+\Phi)^2}\{2v_j p_{at2} + l\gamma_i p_{ar2} - l\gamma_j p_{ar3} - 2v_i p_{at2}\}, \tag{A17}$$

$$(M_e)_{5,4} = \frac{-I_i}{840l^2(1+\Phi)^2}\{2w_j p_{at2} - l\beta_i p_{ar2} - l\beta_j p_{ar3} - 2w_i p_{at2}\}, \tag{A18}$$

$$(M_e)_{5,6} = -(M_e)_{5,1}, \tag{A19}$$

$$(M_e)_{5,7} = -(M_e)_{5,2}, \tag{A20}$$

$$(M_e)_{5,8} = \frac{I_i}{840l(1+\Phi)^2}\{2v_j p_{at3} + l\gamma_i p_{ar2} + l\gamma_j p_{a1} - 2v_i p_{at3}\}, \tag{A21}$$

$$(M_e)_{5,9} = \frac{-I_i}{840l(1+\Phi)^2}\{2w_j p_{at3} - l\beta_i p_{ar2} - l\beta_j p_{a1} - 2w_i p_{at3}\}, \tag{A22}$$

$$(M_e)_{10,1} = \frac{I_i}{420l^2(1+\Phi)^2}\{6w_j p_{t1} - l\beta_i p_{t2} - l\beta_j p_{t3} - 6w_i p_{t1}\}, \tag{A23}$$

$$(M_e)_{10,2} = \frac{-I_i}{420l^2(1+\Phi)^2}\{6v_j p_{t1} + l\gamma_i p_{t2} + l\gamma_j p_{t3} - 6v_i p_{t1}\}, \tag{A24}$$

$$(M_e)_{10,3} = \frac{I_i}{840l(1+\Phi)^2}\{2v_j p_{t2} - l\gamma_i p_2 + l\gamma_j p_1 - 2v_i p_{t2}\}, \tag{A25}$$

$$(M_e)_{10,4} = \frac{-I_i}{840l(1+\Phi)^2}\{2w_j p_{t2} + l\beta_i p_2 - l\beta_j p_1 - 2w_i p_{t1}\}, \tag{A26}$$

$$(M_e)_{10,6} = -(M_e)_{10,1}, \tag{A27}$$

$$(M_e)_{10,7} = -(M_e)_{10,2}, \tag{A28}$$

$$(M_e)_{10,8} = \frac{I_i}{840l(1+\Phi)^2}\{2v_j p_{t3} + l\gamma_i p_1 + l\gamma_j p_2 - 2v_i p_{t3}\}, \tag{A29}$$

$$(M_e)_{10,9} = \frac{-I_i}{840l(1+\Phi)^2}\{2w_j p_{t3} - l\beta_i p_1 - l\beta_j p_2 - 2w_i p_{t3}\} \tag{A30}$$

where

$$\begin{aligned}
p_{at1} &= 18\delta_1 + 9\delta_2 + 5\delta_3 + 3\delta_4 + 42,\\
p_{at2} &= 6\delta_1(7\Phi - 2) + 9\delta_2(2\Phi - 1) + 3\delta_3(3\Phi - 2) + \delta_4(5\Phi - 4) + 126\Phi,\\
p_{at3} &= 6\delta_1(7\Phi - 2) + 3\delta_2(8\Phi - 1) + 15\delta_3\Phi + \delta_4(10\Phi + 1) + 42(2\Phi - 1),\\
p_{ar2} &= 2\delta_1(14\Phi^2 - 14\Phi - 1) + \delta_2(14\Phi^2 - 14\Phi - 1) + \delta_3(8\Phi^2 = 8\Phi - 1)\\
&\quad + \delta_4(5\Phi^2 - 5\Phi - 1) + 14(5\Phi^2 - 5\Phi - 1),\\
p_{ar3} &= -6\delta_1(7\Phi^2 + 2) - \delta_2(14\Phi^2 - 8\Phi + 5) - 3\delta_3(2\Phi^2 - 2\Phi + 1)\\
&\quad - \delta_4(3\Phi^2 - 4\Phi + 2) - 21(10\Phi^2 + 8\Phi + 5),\\
p_{a1} &= 6\delta_1(7\Phi^2 + 2) + \delta_2(28\Phi^2 + 8\Phi + 7) + 5\delta_3(4\Phi^2 + 2\Phi + 1)\\
&\quad + \delta_4(15\Phi^2 + 10\Phi + 14) + 14(5\Phi^2 - 2\Phi + 2),\\
p_{t1} &= 24\delta_1 + 15\delta_2 + 10\delta_3 + 7\delta_4 + 42,\\
p_{t2} &= 6\delta_1(7\Phi - 5) + 3\delta_2(8\Phi - 7) + 15\delta_3(\Phi - 1) + \delta_4(10\Phi - 11) + 42(2\Phi - 1),\\
p_{t3} &= 12\delta_1(7\Phi + 1) + 15\delta_2(4\Phi + 1) + 15\delta_3(3\Phi + 1) + 7\delta_4(5\Phi + 2) + 126\Phi,\\
p_1 &= 6\delta_1(7\Phi^2 - 7\Phi - 2) + \delta_2(28\Phi^2 - 28\Phi 11) + 10\delta_3(2\Phi^2 - 2\Phi - 1)\\
&\quad + 3\delta_4(5\Phi^2 - 5\Phi - 3) + 14(5\Phi^2 - 5\Phi - 1),\\
p_2 &= 4\delta_1(-7\Phi^2 + 7\Phi - 4) - \delta_2(14\Phi^2 - 20\Phi + 11) - 2\delta_3(4\Phi^2 - 7\Phi + 4)\\
&\quad - \delta_4(5\Phi^2 - 10\Phi + 6) - 14(5\Phi^2 - 2\Phi + 2).
\end{aligned}$$